Rheology and self-healing of amine functionalized polyolefins

B. M. Yavitt, T. Tomkovic, D. J. Gilmour, et al.

Citation: Journal of Rheology **66**, 1125 (2022); doi: 10.1122/8.0000364
View online: https://doi.org/10.1122/8.0000364
View Table of Contents: https://sor.scitation.org/toc/jor/66/6
Published by the The Society of Rheology

Rheology and self-healing of amine functionalized polyolefins

B. M. Yavitt,[1,2] T. Tomkovic,[1] D. J. Gilmour,[2] Z. Zhang,[1] N. Kuanr,[2] E. van Ruymbeke,[3] L. L. Schafer,[2,a)] and S. G. Hatzikiriakos[1,a)]

[1]*Department of Chemical and Biological Engineering, University of British Columbia, Vancouver, British Columbia V6T 1Z3, Canada*
[2]*Department of Chemistry, University of British Columbia, Vancouver, British Columbia V6T 1Z4, Canada*
[3]*Bio-and Soft Matter, Institute of Condensed Matter and Nanosciences, Universite Catholique de Louvain, Croix du Sud 1, B-1348 Louvain-la-Neuve, Belgium*

(Received 9 September 2021; final revision received 1 August 2022; published 1 November 2022)

Abstract

The rheological and self-healing behavior of a class of catalytically synthesized amine-functionalized polyolefins is investigated. We demonstrate that these materials possess tunable rheological properties according to the molecular weight and display autonomous self-healing. The linear viscoelastic properties are modeled using a tube-based model developed by Hawke *et al.* [J. Rheol., **60**, 297–310, (2016)] to calculate several model parameters that describe the individual chain dynamics. The self-healing response is described by findings from the reptation model as well as recent theory on associating polymer networks with reversible bonds. The cooperation between experiments, modeling, and theory provide insight into designing new materials with programmable rheological properties and superior self-healing ability.
 https://doi.org/10.1122/8.0000364

I. INTRODUCTION

Associating polymers are an important class of synthetic materials that harness polar functional groups to impart dynamic rheological behaviors toward a wide range of material applications [1]. Among these polar functional groups, the ability of amines to participate in hydrogen bonding and other noncovalent interactions can enable such materials to possess beneficial properties such as enhanced mechanical strength, adhesion, and self-healing ability [2–8]. The applications of associating polymers depend on their mechanical and rheological properties originated from the internal cross-linked network and temporary entanglements [9–16]. The diverse behavior is based on the average time needed for the reversible bond to dissociate (known as the association lifetime, τ_b), the mobility of the chains, and polymer chain architecture [17–20].

Recently, a class of amine-functionalized polyolefins was synthesized using a two-step combination of catalytic hydroaminoalkylation (HAA) and ring-opening metathesis polymerization (ROMP) [21]. Notably, these amine-functionalized materials possessed self-healing behavior that was attributed to the ability of the amine-pendant groups to reversibly form hydrogen-bonded networks. The kinetics of healing was supported by recent theory developed by Stukalin *et al.* for non-entangled polymer networks that predicted the time required for self-healing is a function of the lifetime of associations and the size of the associating chain [22].

To improve our understanding of the origin of self-healing phenomenon and relate it to the characterized rheological properties, we experimentally measure the chain dynamics of these systems and apply modeling using various theoretical approaches [23–25]. In the present work, we have used a comprehensive time-marching algorithm (TMA) developed by Hawke *et al.* where the linear viscoelastic behavior of amine containing polyolefins can be explained by a small number of physical parameters [18,25,26]. This modeling approach provides a feasible determination of molecular model parameters (such as number of entanglements versus number of possible reversible associations) which are useful in understanding the complex dynamics.

In summary, we first present the various structures of amine-functionalized polyolefins synthesized. Next, we study the linear viscoelastic properties (LVE) as fingerprints of the various structures. We use the TMA to model the LVE behavior of these polymers to determine the number of associating groups participating in the network formation and the various relaxation times, such as the Rouse time τ_R governing the dynamics of the individual chains and sticky reptation time $\tau_{rep,S}$ which governs entanglement relaxation. The determination of these parameters is used to explain their dynamic rheological behavior as well as their self-healing behavior.

II. MATERIAL SYNTHESIS AND EXPERIMENTAL METHODOLOGY

A. Polymer synthesis

The amine-functionalized materials investigated herein were prepared according to our previous report of their

Note: This paper is part of the special issue on Double Dynamics Polymeric Networks

a)Authors to whom correspondence should be addressed: schafer@chem.ubc.ca and savvas.hatzi@ubc.ca

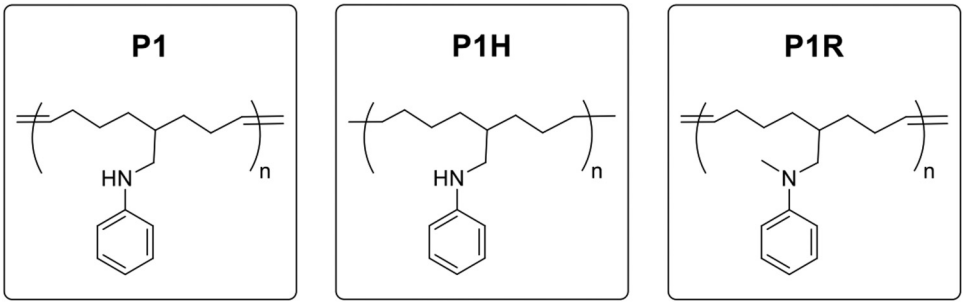

FIG. 1. Various structures synthesized and studied in the present work: functionalized aminated poly(cyclooctene) (**P1**) structure and hydrogenated backbone (**P1H**) structural analog. Unfunctionalized reference sample (**P1R**) with tertiary amine functional group.

synthesis via a two-step catalytic sequence of HAA followed by ROMP (Figure 1) [21]. The base polymer **P1** features a poly(cyclooctene) backbone functionalized with an *N*-methyl aniline derivative. The secondary amine can participate in hydrogen bonding. Amines and anilines have a reported bond dissociation energy (ΔH) on the order of 10 kJ/mol, weaker than that of carboxylic acids ($\Delta H = 30$ kJ/mol) and quadruple hydrogen bonding ureido-pyrimidinone (UPy) groups ($\Delta H = 70$ kJ/mol) which have been studied extensively in the literature [27,28]. To further modify **P1**, reductive hydrogenation of the backbone was performed to yield **P1H**. Upon saturation, **P1H** can be seen as analogous to a linear polyethylene with an amine-pendant branch on every eighth carbon. To obtain a tertiary pendant-amine that is unable to participate in hydrogen bonding, **P1R** was obtained from alkylation of **P1** to produce a reference system that cannot readily form reversible associations. To explore the effect of molecular weight, several different polymers of varying length were prepared by varying the monomer-to-initiator ratio in ROMP (Table I).

TABLE I. Catalog of aminated poly(cyclooctene) derivatives synthesized with reported molecular and thermal characteristics.

Polymer	M_w[a] (kg/mol)	$Đ$[a]	T_g (°C)[b]
P1	18.8	2.10	−12.5
	27.2	1.70	
	57.1	1.47	
	71.5	1.97	
	141.3	4.00[c]	
P1H	22.3	1.73	−17.1
	57.8	1.69	
	87.1	1.22	
P1R	25.4	1.90	−24.7
	50.3	2.70	
	173.3	4.00[c]	

[a]Weight average molecular weight and dispersity index determined by triple detection gel permeation chromatography (GPC).
[b]Glass transition temperatures (T_g) representative for each class of polymer as measured by differential scanning calorimetry (DSC) as previously reported [21]. T_g was determined to be independent of M_w.
[c]The PDI values for the two highest molecular weight polymers are fitted values according to the TMA model, adjusted to be consistent with the low level of the plateau modulus (below the entanglement plateau) suggesting the presence of a larger fraction of shorter chains not captured by GPC. All other PDI values from GPC are consistent with the model predictions.

B. Rheological measurements

The rheological measurements were performed using a stress-controlled rotational rheometer (Anton Paar, MCR702) equipped with 25 mm parallel plate and 8 mm cone-partitioned plate which is capable of delaying the formation of edge fracture and other instabilities to higher deformation rates well within the nonlinear viscoelastic regime [29–32]. Air/nitrogen convection oven was used for temperature control with accuracy of ±0.1 °C. Dynamic time sweep tests were done in advance at each temperature ($T = 30$–90 °C) with an angular frequency of $\omega = 0.1$ Hz and strain $\gamma = 0.01$ to determine the thermal stability and equilibrium of polymers. Over a period of 2 h, there was no change in the complex modulus indicating no change in structure and adequate thermal stability. The linear viscoelastic region was determined from an oscillatory strain sweep by applying a constant frequency of $\omega = 0.1$ Hz at the reference temperature of $T = 30$ °C. Lastly, the frequency sweep test was conducted over a wide range of angular frequency ($\omega = 0.1$–100 rad/s) at several temperatures ($T = 30$–90 °C) at 20 °C intervals and strain of $\gamma = 0.01$.

The time-Temperature superposition (tTS) principle was applied to construct the master curves of storage (G'), loss moduli (G''), and complex viscosity (η^*) of all polymers synthesized. These polymers are generally thermorheologically simple and only horizontal shift factors a_T were used to obtain the master curves.

The ability of self-healing of **P1** and **P1H** was demonstrated by performing tensile tests using SER2 (Xpansion instruments) fixture on the rheometer at room temperature without employing any external stimuli, such as pressure, heat, or solvent [33]. Rectangular samples of dimensions $1.5 \times 1.0 \times 0.3$ cm^3 were prepared. The experimental procedure consists of the following steps: first, the stress–strain curve of the pristine sample was recorded at room temperature under a constant Hencky strain rate of $\dot{\varepsilon} = 0.005$ s^{-1}. The sample was subsequently cut into two pieces before its parts were gently brought into complete interfacial contact in the absence of any external stimuli (such as temperature or significant pressure). The waiting time (t_w) between cutting and reassembly was on the order of a few seconds. After visual inspection of the flush interfacial contact, the two sections were allowed to heal for different healing times ($t_h = 5$–120 min) at ambient conditions. Finally, the stress–strain curve was recorded under the same conditions as in the

case of the pristine sample. The cycle of stretching, breaking, and healing was performed numerous times using the same t_w and t_h conditions to verify repeatability.

III. RESULTS AND DISCUSSION

A. Linear viscoelasticity of unfunctionalized polymers

Figure 2 shows the master curves of G' and G'' for three **P1R** (nonassociating reference polymers) of various molecular weights listed in Table I. The samples show typical behavior of entangled polymers such as a rubbery plateau followed by a crossover between the storage and loss moduli [34]. The small side groups in **P1R** suppress the crystallization typically found in polyolefins and provide the flexibility for entanglement formation. At low angular frequency, **P1R** polymer attains terminal relaxation where $G' \sim \omega^2$ and $G'' \sim \omega^1$. The TMA algorithm was used to fit the data to determine the model parameters of these samples, i.e., the molecular weight between two entanglements ($M_e = 7000$ g/mol), the plateau modulus $\left(G_N^0 = \frac{4}{5}\rho RT/M_e = 0.35 \text{ MPa}\right)$, and equilibration time of an entanglement segment, τ_e. The modeling indicates that the **P1R** polymers create about $Z_E = M_w/M_e = 3.5$, 7.2, and 24.7 entanglements per chain on average [24]. The Rouse (τ_R) and reptation (τ_{rep}) times can be calculated using τ_e according to the scaling relationships $\tau_R = Z_E^2\tau_e$ and $\tau_{rep} = 3Z_E\tau_R$. The model fit parameters (listed in Table II) τ_e, G_N^o, M_e are used to inform the analysis of the associating polymers below.

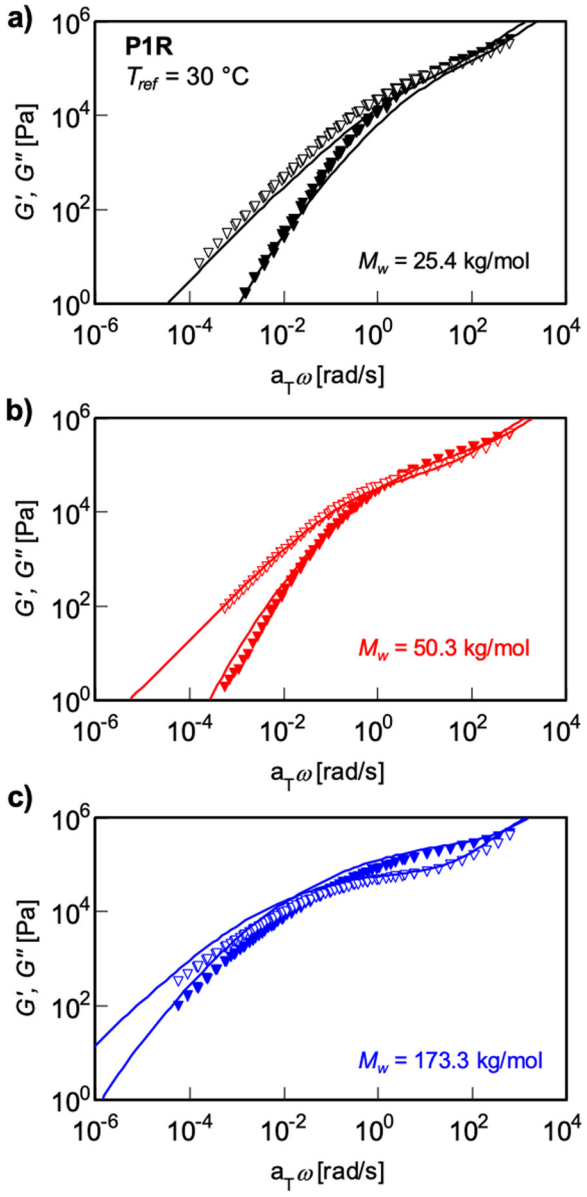

FIG. 2. Master curves of storage (closed symbols) and loss moduli (open symbols) for nonassociating reference samples **P1R** with varying M_w at reference temperature of $T_{ref} = 30$ °C. Lines show fit of TMA to the experimental data used to determine material parameters. (a) $M_w = 25.4$ kg/mol, PDI = 1.9 (black curve), (b) $M_w = 50.3$ kg/mol, PDI = 2.7 (red curve), and (c) $M_w = 173.3$ kg/mol, PDI = 4.0 (blue curve).

While the **P1R** polymers were found to be thermorheologically simple, it is well known that associating polymers may be thermorheologically complex due to divergent temperature dependencies of segmental motion and hydrogen bonding. A van Gurp-Palmen (vGP) plot of **P1** polymer is shown in Fig. 3(a) to validate the application of the time-Temperature Superposition (tTS) principle. Overall, the aminated polyolefins generally follow tTS. We observe some deviation in the overlap of vGP, especially for the higher M_w samples, clearly reflecting the anticipated competition between the chain dynamics and hydrogen bonding. Horizontal shift factors determined by tTS were used to construct the master curves and found to follow a WLF dependence as $\log(a_T) = -C_1(T–T_0)/(C_2 + T–T_0)$ shown in Fig. 3(b) at the reference temperature of $T_0 = 30$ °C (303 K). Here, we plot $\log(a_T)$ vs temperature normalized to the glass transition temperature, T_g, $(T–T_g)$ reported in Table I. The associating structures **P1** and **P1H** show similar temperature dependent behavior due to the proximity of their T_g. However, there are differences in the WLF fits through the experimental data, which are represented by the dashed lines in Fig. 3. The WLF parameters for each sample are as follows: **P1**-$C_1 = 15.49$, $C_2 = 280.3$ K, **P1H**-$C_1 = 7.93$, $C_2 = 102.3$ K, and **P1R**-$C_1 = 5.59$, $C_2 = 75.6$ K.

B. Linear viscoelasticity of functionalized polymers

The linear viscoelasticity of **P1** samples at various M_w are compared below. The number of intermolecular associations formed by hydrogen bonding influence the linear viscoelastic behavior of these polymers by various degrees [17,25,28,35,36]. Figure 4(a) depicts the storage modulus and Fig. 4(b) the loss modulus of **P1** (from poorly to well entangled) at different molecular weights ranging from $M_w = 18.8$ kg/mol to $M_w = 141.3$ kg/mol. At high angular frequency, all curves merge as the dynamics of these polymers are controlled by the relaxation of segments between entanglements/associations (number of associations, Z_S and number of entanglements, Z_E). The equilibration time for **P1** ($\tau_e = 12 \times 10^{-3}$ s) is different from **P1R** due to the difference in T_g between each polymer. τ_e is labeled on Fig. 4 accordingly and is consistent for frequencies $\omega > \frac{1}{\tau_e} = 83.33$ rad/s where the data from each sample merge together following Rouse time relaxation scaling ($G', G'' \sim \omega^{1/2}$) [37]. The rubbery plateau of these associating polymers is comparable to the value found for the nonsticky entangled sample

TABLE II. Parameters of the TMA model. τ_{Rouse}, τ_{rep}, $\tau_{sticker}$, and $\tau_{rep\text{-}sticky}$ reported in units of seconds.

P1	$M_e = 7000$ g/mol, $G_N = 0.35$ MPa, $\tau_e = 12 \times 10^{-3}$ s			$M_{xx} = 500$ g/mol, $p_{free} = 0.99$		
M_w (kg/mol)	Z_e	τ_{Rouse}	τ_{rep}	Z_s	$\tau_{sticker}$	$\tau_{rep,S}$
18.8	2.69	0.09	0.70	37.6	3	814
27.2	3.89	0.18	2.11	54.4	3	2466
57.1	8.16	0.80	19.5	114	3	22 815
71.5	10.2	1.25	38.4	143	3	44 796
141.3	20.2	4.90	296	282	3	345 743
P1H	$M_e = 7000$ g/mol, $G_N = 0.35$ MPa, $\tau_e = 6.5 \times 10^{-3}$ s			$M_{xx} = 500$ g/mol, $p_{free} = 0.999$		
M_w (kg/mol)	Z_e	τ_{Rouse}	τ_{rep}	Z_s	$\tau_{sticker}$	$\tau_{rep,S}$
22.3	3.19	0.07	0.63	44.6	0.3	136
57.8	8.26	0.44	11.0	116	0.3	2375
87.1	12.4	1.01	37.6	174	0.3	8128
P1R	$M_e = 7000$ g/mol, $G_N = 0.35$ MPa, $\tau_e = 6 \times 10^{-3}$ s					
M_w (kg/mol)	Z_e	τ_{Rouse}	τ_{rep}			
24.5	3.5	0.07	0.77			
50.3	7.2	0.31	6.68			
173.3	24.7	3.68	273			

($G_N = 0.35$ MPa). Strong associating systems (such as ionic aggregates or quadruple hydrogen bonding UPy) which have comparable energy (k_bT) as entanglements will increase the plateau value at the timescales where associations behave as permanent cross-links, sometimes leading to a second plateau depending on the values of τ_b and τ_e [28,38,39]. However, this enhancement phenomenon is minimized in **P1** due to the weak H-bonding strength of the amine associations.

At the lower frequencies, the effects of associations are significant based on the data plotted in Fig. 4 as well as the data of complex viscosity [$\eta^*(\omega)$] plotted in Fig. 5(a). When comparing within the **P1** series, as the M_w increases above $M_w = 27.2$–71.5 kg/mol (an increase by ~2.6 times), the terminal relaxation time of the samples increases significantly. While the zero-shear viscosity cannot be determined anymore, $\eta^*(\omega)$ at low frequencies increases by a factor of 10^3 which is much higher than the predicted reptation time scaling of $\tau_{rep} \sim M_w^{3.4}$ according to unassociated (simply entangled) linear polymers [which would show a predicted factor of $\sim(2.6)^{3.4}$ ~28]. The significantly longer terminal relaxation time is driven by the introduction of "sticky" reptation [38]. For the highest molecular weight, little relaxation has occurred at time scales of 10^5 s (several hours). The **P1** structure at a M_w as small as $M_w = 27.2$ kg/mol shows terminal relaxation at time scales of the order of $t = 10^3$ s. Comparing this with the reptation time of $\tau_{rep} = 0.77$ s determined for structure **P1R** ($M_w = 24.5$ kg/mol), it can be concluded that the number and effects of reversible associations (hydrogen bonding) become quite significant in the aminated polyolefins. Since these samples only vary by their molecular weight, a synergetic effect of the stickers on the sample relaxation is expected. Molecular weight is clear design parameter

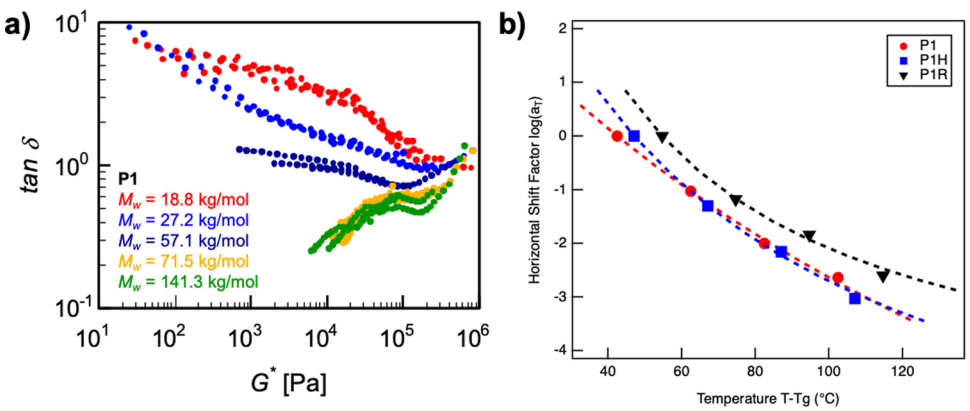

FIG. 3. (a) van Gurp-Palmen plot of **P1** polymers with varying M_w. Overlapping of the linear viscoelastic data suggests applicability of time-temperature superposition principle. Deviations in overlap begin to emerge in higher M_w samples due to competition between chain dynamics and hydrogen bonding. (b) Temperature dependence of the horizontal shift factors (a_T) used to construct the master curves for each sample ($T_0 = 30$ °C). Dashed line represents the WLF equation fitting to each sample data.

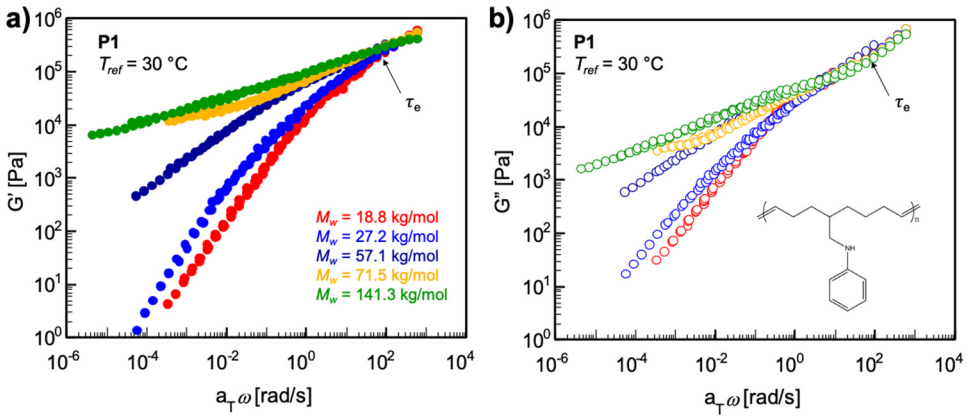

FIG. 4. The master curves of (a) storage modulus $G'(\omega)$ and (b) loss modulus $G''(\omega)$ of polymer **P1** with different molecular weights at the reference temperature of $T_{ref} = 30$ °C.

to control the liquid-like, gel-like, and solid-like behavior of the aminated polyolefins, which lend them to an array of different applications that require modular flow properties.

Figure 5(b) shows the master curves of complex viscosity $[\eta^*(\omega)]$ for the **P1H** polymers with different molecular weights. The characteristic shape of η^* for **P1R** is analogous to the **P1**, as well as the rapid increase in zero-shear complex viscosity with M_w is also observed for the **P1H**. Figure 6 further compares the dynamics of **P1**, **P1H,** and **P1R** structures at comparable molecular weights at a reference temperature of $T_{ref} = 30$ °C. The pendant groups in both structures in **P1** and **P1H** are identical. Therefore, the only chemical difference is the absence of a carbon double bond in the backbone of the **P1H** structure, resulting in a decreased T_g relative to **P1** structure ($T_g = -17.1$ °C of **P1H** vs $T_g = -12.5$ °C of **P1**). The impact of T_g on the chain dynamics is considered in the modeling section, where the τ_e are defined as 6×10^{-3}, 6.5×10^{-3}, and 12×10^{-3} s for the samples **P1R**, **P1H**, and **P1**, respectively.

As seen from Fig. 6, similar dynamics are exhibited by these two classes of polymers with the **P1H** structure polymers relaxing relatively faster, supposedly due to an increase in chain flexibility. If **P1H** backbone is indeed more flexible, one could expect a change in entanglement structure with a decrease in M_e, increase in G_N, and increase in relaxation time from entanglements. However, to the best of our ability, we find that all sticky samples have a similar plateau ($G_N = 0.35$ MPa), which is the same as the plateau of the reference samples **P1R**. Chain flexibility can be evaluated according to the packing length (p) of the polymer chain [40]. A change in p by chemical modification to the monomer volume v_0 or Kuhn length b results in a new average packing length $\bar{p} = av_0/b^2$. Shabbir *et al.* found that this new packing length will result in a new $G_N = G_{N,0}/\alpha^3$ and $\tau_{rep} = \tau_{rep,0}/\alpha^{6.8}$ [17]. Hydrogenation of the olefin backbone from **P1** to **P1H** should not drastically impact v_0 (due to the minimal change in monomer molar mass m_0) but will lead to a slight increase in b as poly(cyclooctene) (backbone of **P1**) has $b = 1.4$ nm compared to polyethylene (backbone of **P1H**) which has a $b = 1.54$ nm [40,41], The resulting decrease in the new packing length (i.e., $\alpha < 1$) of **P1H** is not enough to significantly increase G_N according to the weak dependency with α compared to the stronger dependency of τ_{rep}. Therefore, we find that the plateau is due to the chain entanglements and not heavily impacted by chemical transformation of the backbone. Due to the weak association energy, the presence of the stickers does not affect the value of G_N, only the relaxations at timescales beyond the entanglement plateau.

The dynamics of **P1** and **P1H** converge in the high frequency regime due to the similar G_N, where the polymers are

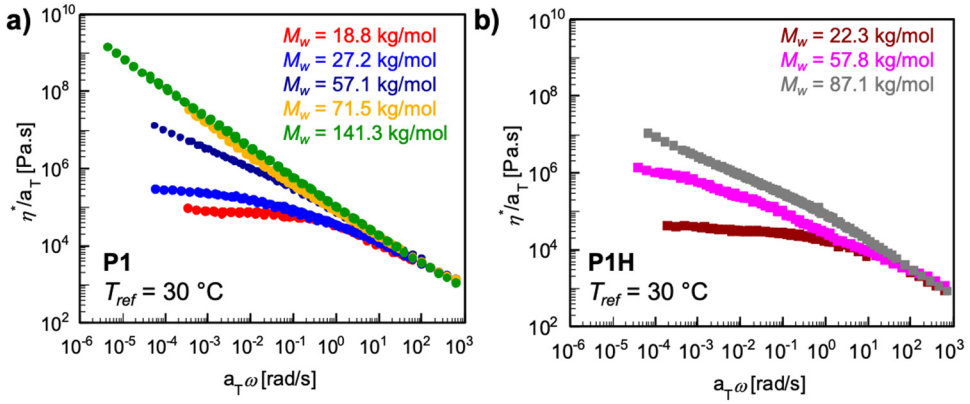

FIG. 5. Master curve of complex viscosity $[\eta^*(\omega)]$ of (a) **P1** and (b) **P1H** with different molecular weights constructed via tTs using a reference temperature of $T_{ref} = 30$ °C.

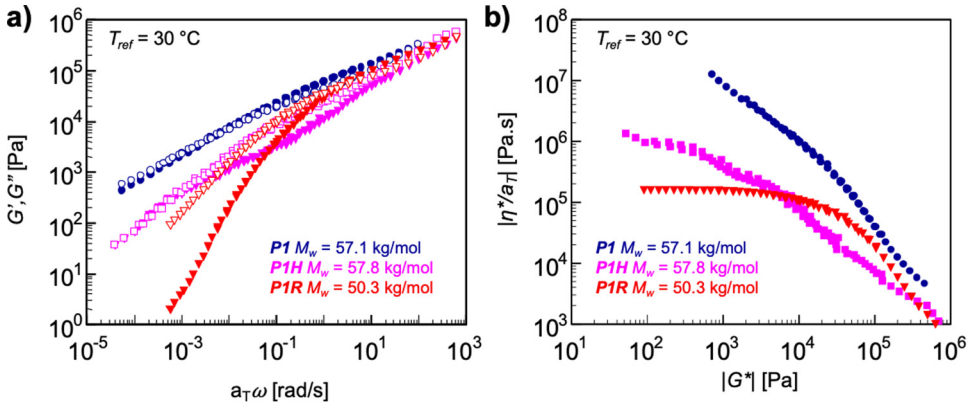

FIG. 6. (a) Master curves of storage G' (closed symbol) and loss G'' (open symbols) moduli at reference temperature of $T_{ref} = 30\,°C$ for **P1**, **P1H**, and **P1R** samples of comparable M_W. (b) Complex viscosity (η^*) vs complex modulus (G^*) at reference temperature of $T_{ref} = 30\,°C$ for **P1**, **P1H**, and **P1R** samples of comparable M_W.

stiff (G', $G'' \sim 10^6$ Pa); however, the Rouse relaxation dynamics of **P1H** is found to be about two times faster than **P1** due to the T_g difference and acceleration of sticky timescales. The impact of the hydrogenation in **P1H** on the relaxation timescales is especially apparent at lower frequencies when the polymers are softer and liquid-like compared to **P1**. The relative liquid/solid-like response are shown in Fig. 6(b) for **P1** samples (circles) and for **P1H** samples (square) and **P1R** (triangle) with similar molecular weights, in a plot of complex viscosity (η^*) vs complex modulus (G^*), where horizontal curves correspond to liquid-like behavior and vertical curves correspond to solid-like behavior [42]. **P1R** reaches a horizontal plateau in complex viscosity, indicating terminal relaxation. The **P1** sample shows a steeper vertical curve to very high viscosity values ($\eta^* > 10^8$ Pa s) suggesting much more solid-like behavior compared to **P1H** at this M_w, which slowly transitions to the vertical solid limit.

C. Modeling of linear viscoelastic behavior

To describe the viscoelastic properties of **P1** and **P1H**, one must determine the number of active stickers along the backbone, $Z_s = M_w/M_{xx}$, where M_{xx} is the molecular weight between two active stickers [25,32,35,36,43,44]. Cates *et al.* presented a comprehensive model for the dynamics of supramolecular networks based on reversible scission and recombination of associations [23,24], but recent experimental studies have shown qualitative and quantitative limitations [45,46]. Further extension to Rouse and reptation based models provide scaling laws that relate the relaxation times and viscoelastic parameters to the number of reversible associations and entanglements [24,35,36]. Here, we use the time-marching algorithm (TMA) which is a tube-based reptation model capable of predicting the LVE behavior of entangled polymers with various architectures such as linear and star polymers. The TMA model has also been extended to describe the dynamics of associating polymers [25,26,43,47].

Various chain dynamic parameters (M_e, G_N^0, and τ_e) were determined by modeling the unassociated reference polymer **P1R**. As previously mentioned, the same values of G_N^0 and M_e have been used for the **P1** and **P1H** samples. Hydrogenation has a stronger impact on T_g, which is expressed in the chain dynamics by defining τ_e as 6×10^{-3}, 6.5×10^{-3}, and 12×10^{-3} s for the samples **P1R**, **P1H**, and **P1**, respectively. To describe the viscoelastic properties of the associating chains using the TMA, three remaining parameters must be resolved: M_{xx}, which is the average molar mass between two reversible associating crosslinkers, p_{free}, which determines the delay effect of the crosslinkers on the contour length fluctuation (CLF) process, and $\tau_{sticker}$, which determines the delay effect of the crosslinkers on the reptation process. Based on the value of M_{xx}, the probability that a monomer along the chain is an effective sticker is determined as $p_{sticker} = 1/(M_{xx}/m_0)$, with m_0 being the monomeric molar mass ($m_0 = 215$ g/mol for **P1**). The relaxation modulus is $G(t) = G_{Rouse}(t) + G_N^0 . \varphi(t)\phi_{tube}(t)$, where $G_{Rouse}(t)$ accounts for the high frequency Rouse relaxation, $\varphi(t)$ represents the survival fraction of initial tube segments (not relaxed by reptation or contour length fluctuations) at time t, and the dilation factor $\phi_{tube}(t)$ takes into account the constraint release process and is described in Ref. 25.

The relaxation of the sticky chains can only occur at the rhythm of the dissociation/association of the latter. Therefore, following the sticky reptation model [24], the corresponding reptation time $\tau_{rep,S}$ in Eq. (1) is determined by considering extra friction points along the backbone, to account for the slower dynamics of the stickers,

$$\tau_{rep,S} \approx \frac{a^2 Z^2}{kT}\left(\zeta_0 N_e Z + Z_s \frac{kT}{\frac{a^2}{\tau_s}}\right) = 3\,\tau_e\,Z^3 + Z_s\,\tau_s Z^2, \quad (1)$$

where a is the tube diameter, ζ_0 is the monomeric friction, N_e is the number of Kuhn segment in an entanglement segment, Z_S is the number of stickers along the chain, and delay factor τ_s (i.e., $\tau_{sticker}$) is a function of the lifetime of associations. Furthermore, the sticker activity also slows down the chain relaxation by CLF. It is expected that the delay on the relaxation of a chain segment x, from $x = 0$ at the extremity to $x = 1$ in the middle of the chain, increases with the number of stickers, N_{st}, located between x and the closest chain extremity, i.e., $N_{st}(x) = \frac{Z_s}{2}\,x$. Assuming that

the dissociation of the stickers must be coordinated to allow the molecular segment to relax, Eq. (2) considers that the penalty on the fluctuations time increases exponentially with this number,

$$\tau_{fluc-sticky}(x) = \frac{1}{p_{free}^{N_{st}}}\ \tau_{fluc}(x), \qquad (2)$$

where $\tau_{fluc}(x)$ is the fluctuation time of x in the absence of stickers and p_{free} is a new parameter which represents the probability that a sticker will allow contour length fluctuations which can range from $p_{free} = 0$ (CLF are restricted) to $p_{free} = 1$ (CLF are allowed).

There are several combinations of M_{xx}, p_{free}, and $\tau_{sticker}$ which can describe the data. For example, a lower density of crosslinks (i.e., a larger value of M_{xx}) can be compensated by a stronger delay effect of the latter (thus, a lower value of p_{free} and a larger value of $\tau_{sticker}$). **P1**, **P1H**, and **P1R** have a similar rubbery plateau, suggesting that the presence of the stickers does not affect the value of M_e. We also use the same value of M_{xx} for both the **P1** and **P1H** samples as the association chemistry does not vary between these two. Theoretically, the maximum number of associations can be calculated for these polymers as each monomer (of about 215 g/mol) contains a sticker. However, for entropic reasons, it is unlikely for each repeating unit to form reversible associations [17,25,48]. Furthermore, it is expected that the chains contain a non-negligible fraction of intramolecular associations, leading to the formation of several ineffective, unentangled loops. We propose that two consecutive monomers cannot be associated simultaneously, so M_{xx} is fixed at 500 g/mol, or approximately every other monomer, for both the **P1** and the **P1H** samples. Due to the high density of stickers and the low association energy, it is more reasonable to consider many stickers with shorter lifetimes than a few stickers with long lifetime in these polymers. p_{free} and $\tau_{sticker}$ describe the relaxation of the sticky chains. We impose that the fit parameters do not depend on the total M_W and, therefore, stays constant for all the samples of a same family (either **P1** or **P1H**), as the chemistry and, therefore, chain flexibility is equivalent. The values of p_{free} and $\tau_{sticker}$ are then modulated by a best-fitting procedure until the fits are appropriate for all **P1** and **P1H** samples in each series, respectively.

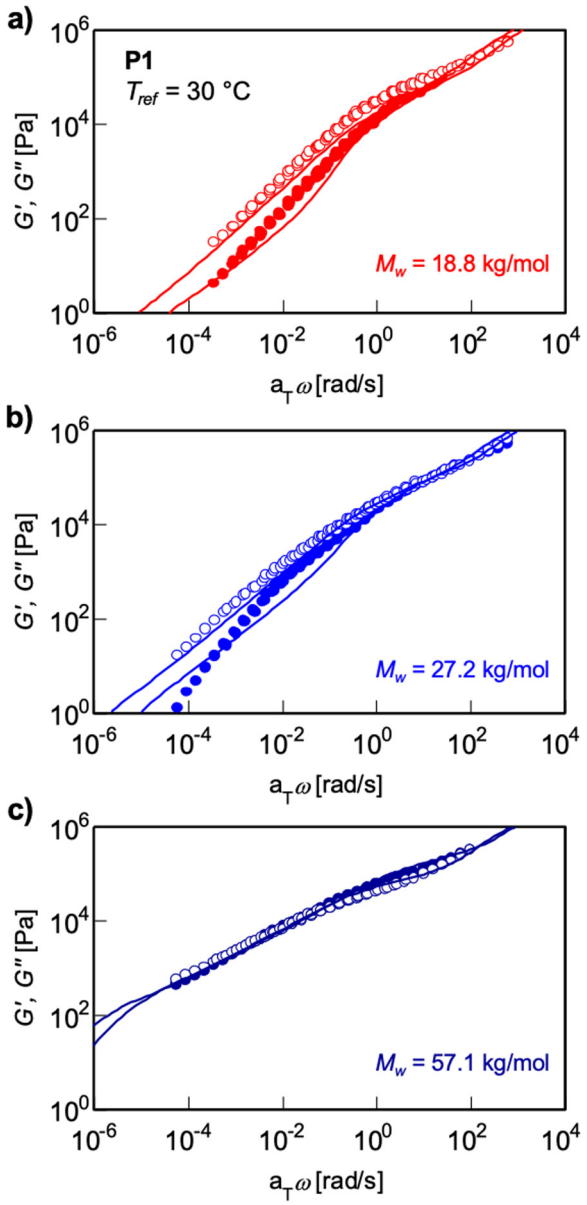

FIG. 7. Comparison between the TMA model and experimental data of storage (closed symbols) and loss moduli (open symbols) at $T_{ref} = 30$ °C for **P1** polymers of relatively low M_w (a) 18.8 kg/mol (red curve), (b) 27.2 kg/mol (blue curve), and (c) 57.1 kg/mol (purple curve).

Figure 7 compares the model fits (parameters listed in Table II) with the LVE experimental data for the **P1** polymers of lower M_w (18.8, 27.2, and 57.1 kg/mol). The model captures the dynamics of these polymers quite well where $\tau_e = 12 \times 10^{-3}$ s is used for **P1**. The slow relaxation of associating polymers is quantitatively revealed as the new $\tau_{rep,S}$ is a factor of 1.1×10^3 times longer than the corresponding τ_{rep} for the chain. The sticker lifetime was found to be $\tau_{sticker} = 3$ s. The latter value should not be taken as the "real lifetime" of the sticker but rather describes a global influence of the sticker on the chain dynamics and strongly depends on the ability of a dissociated sticker to diffuse in the melt and find a new sticky partner. The final fit parameter has been determined as $p_{free} = 0.99$ which essentially means that the efficiency of the relaxation by contour length fluctuations remains constant for stickers between the chain extremity and the segment that is trying to relax. A large value of p_{free} indicates a larger probability for a sticker to be free. In these polymers with a high density of amine groups, while rapidly active association and dissociation events of a specific sticker have a negligible effect on CLF (as reflected by the large value of p_{free}), the cumulative effect of all these amine groups can significantly slow down CLF. On the other hand, one would expect CLF to be locally suppressed when strong stickers with long lifetimes are used.

Figure 8 compares the model predictions (parameters listed in Table II) with the LVE experimental data for the **P1** polymers of relatively higher M_w (71.5 and 141.3 kg/mol). It is observed that using the same parameters as those used in Fig. 7 for the lower M_w samples allows correct capture of the

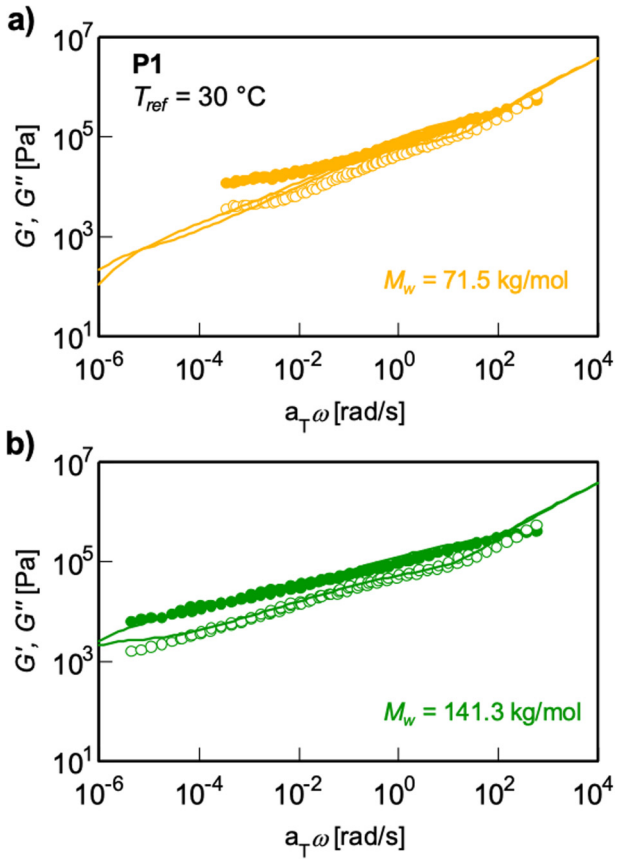

FIG. 8. Comparison between the TMA model and experimental data of storage (closed symbols) and loss moduli (open symbols) at $T_{ref} = 30$ °C for **P1** polymers of relatively high M_w (a) 71.5 kg/mol and (b) 141.3 kg/mol.

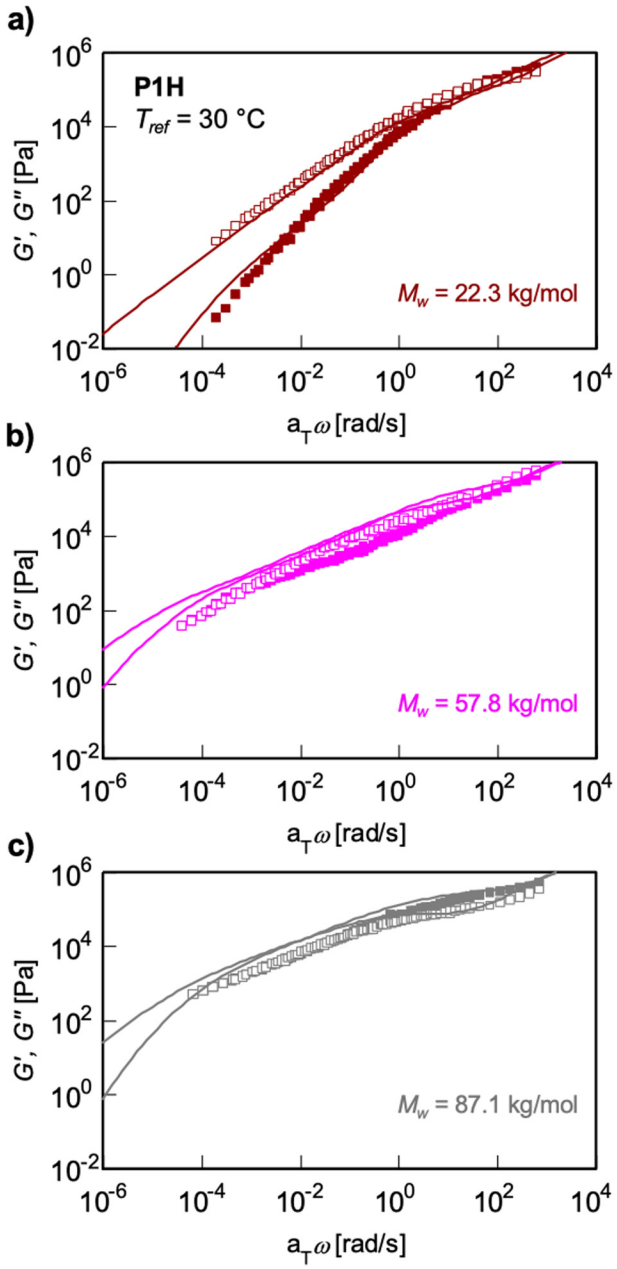

FIG. 9. Comparison between the TMA model and experimental data of storage (closed symbols) and loss moduli (open symbols) at $T_{ref} = 30$ °C for **P1H** polymers (a) 22.3 kg/mol (maroon curve), (b) 57.8 kg/mol (pink curve), and (c) 87.1 kg/mol (gray curve).

high and intermediate frequency data; however it leads to a faster terminal relaxation prediction compared to the experimental data. The low frequency data are challenging to capture with the model. A possible explanation for this discrepancy is related to the fact that increasing the length of the chains also increases the fraction of stickers located further from the chain extremities. Therefore, when such stickers dissociate, they have a large probability to stay trapped between two associated sticker constraints, which leads to a reduced mobility to diffuse and find another free sticker. In such conditions, the probability to attach back to the same sticker is much larger than the probability in a shorter chain. Overall, prediction of these higher M_w samples is difficult. This could also be due to the presence of associative aggregates or a few long lifetime stickers which may not be captured by the modeling and impacts the homogeneity of the behavior [6,49,50].

Figure 9 compares the theoretical model fits and experimental data for the **P1H** polymers (parameters listed in Table II). As already mentioned, a shorter equilibration time is considered to account for the observed decrease of T_g, $\tau_e = 6.5 \times 10^{-3}$ s. It has been observed in Sec. II (see Fig. 6) that **P1H** relaxes faster than **P1** with a similar molecular weight, where $\tau_{\mathrm{rep,S}}$ is now a factor of 2×10^2 times longer than τ_{rep}. According to our model, this reduced terminal relaxation time can come either from shorter lifetime of the stickers or from a lower density of active stickers. Since the plateau modulus G_N^0 is comparable between **P1** and **P1R**, we keep M_e and M_{xx} constant. Therefore, it is expected that a larger value p_{free} and lower value of $\tau_{sticker}$ is used for the flexible backbone of **P1H**. We find from the best fits that p_{free} increases to 0.999 while $\tau_{sticker} = 0.3$ s, signaling that **P1H** experiences less chain friction and can relax faster than **P1** by both reptation and CLF mechanisms. Hydrogenation of the backbone to a pure polyethylene analog in **P1H** does not appear to impact the overall stiffness of the material system or the entanglement/association structure but accelerates the sticky chain timescales by an order of magnitude. This simple chemical modification could be a useful design parameter toward more programmable rheological properties in this class of associating polymers.

D. Self-healing

Hydrogen bonding has been shown to improve the mechanical strength, while in some cases also enabling self-healing in low T_g materials [51,52]. We hypothesized that by combining hydrogen-bonding interactions with high chain mobility, the aminated materials synthesized in this work will demonstrate strong and fast self-healing on a macroscopic scale. In our previous investigation of amine containing polymers, self-healing was observed between the surface boundaries of two discrete, vacuum-dried polymer spheres when placed into contact at room temperature under ambient conditions. With no externally applied stimuli (neither heat nor pressure), the spheres became coherent and after 24h, no clear boundary between the spheres was found [21]. Healing was attributed to the promotion of chain association by attractive and reversible hydrogen bond interactions between mobile polymer chains (either free or dangling ends) present on the surface. As no chemical modification or reaction is taking place, this property is reversible, and tearing/healing can be repeated. While recovery at ambient conditions in possible, Hinton *et al.* showed that the reapplication technique (such as the applied force) to ensure complete interfacial contact impacts the self-healing in associating polymers [53]. Therefore, we take careful consideration to confirm that the entire interfacial area of the cut samples has reconnected after the waiting time (t_w) of a few seconds.

Here, we demonstrate self-healing in **P1H** alongside **P1** and expand the self-healing dynamics within the theoretical framework of Stukalin *et al.* and Hinton *et al.* [22,53]. Figure 10 displays self-healing resolved by tensile measurements as stress–strain curves [54] at different healing times for two **P1** and two **P1H** samples of low and high M_w. The scales of the vertical and horizontal axis have been kept the same to compare the differences between the material responses. As the healing time t_H increases, the polymers recover their mechanical properties. The lower molecular weight **P1** [Fig. 10(a)] fully recovers its mechanical properties within 20 min, while the higher molecular weight **P1** [Fig. 10(b)] within 60 min. Similar observations can be made by comparing the polymers with **P1H** structure [Figs. 10(c) and 10(d)]. Namely, the low molecular weight **P1H** [Fig. 10(c)] fully recovers its mechanical properties remarkably quick within 10 min, while the higher molecular weight **P1H** [Fig. 10(d)] completely recovers within 120 min (2h).

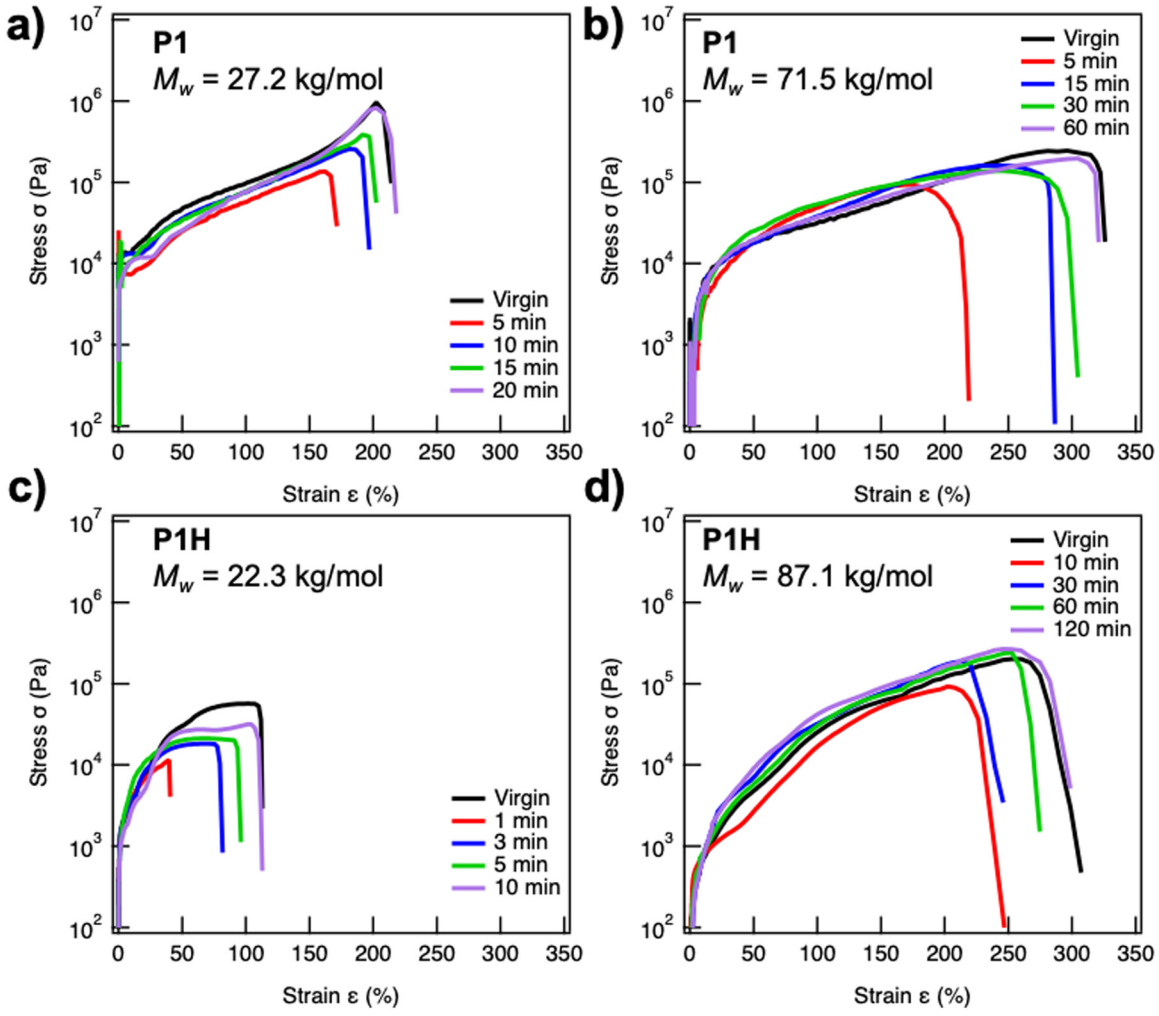

FIG. 10. Self-healing at room temperature of (a) **P1** $M_w = 27.2$ kg/mol, (b) **P1** $M_w = 71.5$ kg/mol, (c) **P1H** $M_w = 22.3$ kg/mol, and (d) **P1H** $M_w = 87.1$ kg/mol. Cut parts were brought into contact after being cut at room temperature (t_w of several seconds). Mechanical testing by stress–strain curves were performed after various healing times designated in the legend.

Notably, low M_W **P1H** structures self-heal faster compared to **P1** polymers supposedly due to their faster relaxation through sticky reptation as discussed above (see Table II). This carries over to the higher mobility (faster diffusion) of the smaller free chains at the interface as well. The actual self-healing time of the high M_W **P1H** sample is only slightly larger than the self-healing time of the high M_W **P1** sample as it does not need the full 120 min to recover its initial extensibility. According to Fig. 10(d), high M_W **P1** nearly behaves as the original sample after just 60 min. Ultimate elongational strain (strain at the failure point), ϵ_u at the constant applied Hencky strain rate increases with M_w irrespective of the structure (**P1** and **P1H**). Specifically, the higher molecular weight polymers [Figs. 10(b) and 10(d)] sustain deformations up to linear elongations of more than 300%, while the polymers with lower molecular weights [Figs. 6(a) and 6(c)] can sustain deformations up to strains slightly higher than 100%. Similar results have been recently reported by Sbrescia *et al.* for block copolymer-based thermoplastic elastomers (TPEs) where higher M_w samples were able to retain more stress bearing units during nonlinear extension, which resulted in a higher stress response and network elasticity [55]. Longer chains produce more total stickers and entanglements which provide a stronger cohesion between chains. Therefore, an interesting indirect trade-off between self-healing and ultimate elongation arises and should be considered when designing future materials.

One may expect that by allowing enough time any material with low T_g is capable of self-healing. For nonassociating polymer, self-healing if facilitated though recovery of the entanglements at the interface, of which the timescale is defined by reptation and diffusion of the chains. Full recovery of mechanical properties was not observed in **P1R** after maintaining contact over the timescale of t_H used for **P1** and **P1H**, highlighting the importance of association re-establishment at the interface to regain mechanical strength.

Stukalin *et al.* presented a theory of self-healing for unentangled polymer networks [22]. When a new interface is created by cutting the sample, the interfacial structure evolves as severed associations move to find new partners. The ability for the interface to reheal is a function of the waiting time, t_w, before surfaces are reconnected. For example in unentangled chains, if $t_w < \tau_R$, the dangling ends do not diffuse away from the surface and rehealing goes to a subequilibrium state [22]. This evolution is dependent on τ_b as well. If $t_w < \tau_b$, dangling ends will diffuse away but not exchange with their partners and therefore recovery is minimal. When $t_w > \tau_b$, chains can exchange and recover. While no complete self-healing theory exists for entangled associating networks, aspects of Stukalin's theory can be used in the present work to establish a regime of self-healing based on important timescales, both from a chain and associative dynamics perspective. Hinton *et al.* presented application of the theory to describe self-healing in entangled acrylate polymers from the aspect of relaxation (τ_R, τ_{rep}) and associative timescales where τ_b and equilibration time τ_{eq} plays a role in concert with the reptation dynamics [53]. $\tau_b \approx \tau_0 \exp(\varepsilon/k_BT)$ is the average time two stickers spend in a bonded state before a successful separation and is governed by the sticker equilibration time τ_0 and the bond strength ε, estimated to be 10 kJ/mol for secondary amines [27]. $\tau_{eq} = [(\tau_0/N)\exp(3\varepsilon/2k_BT)]$ is the time for open stickers to reach equilibrium within the network and is a function of the number of monomers in a sticky group N (~2 in the case of **P1** and **P1H**). Both **P1** and **P1H** feature a significantly high number density of weaker associations with association timescales of $\tau_b = 2.7 \times 10^{-3}$ s and $\tau_{eq} = 6.4 \times 10^{-1}$ s for **P1** and $\tau_b = 1.5 \times 10^{-3}$ s and $\tau_{eq} = 3.5 \times 10^{-1}$ s for **P1H.** The association timescales are fast relative to t_w (~1 s) and t_h (~100 s). The large collection of weak bonds results in fast exchange timescales and quick equilibration at the cut interface and is considered a regime of self-adhesion according to Stukalin *et al.* [22]. In this regime, recovery is independent of t_w. Hinton *et al.* identified that t_h normalized by the characteristic relaxation time for the chains λ (which in this case could be taken as the reptation time) shows a transition point at $t_h/\lambda > 10$. Re-entanglement dynamics across the interface switch to a regime dominated by reassociation of open groups that contribute to additional recovery of the mechanical properties. With t_{rep} ~1–10 s according to Table II, the drastic recovery observed in Fig. 10 is due to the additional reassociations after entanglement recovery. The effect of strain rate and Weissenberg number $\left(Wi = \dot{\varepsilon}\lambda\right)$ on self-healing dynamics in associating polymers is important to consider as one can probe various contributions from entanglement and associative recoveries by changing *Wi*. Strain rate is kept constant at $\dot{\varepsilon} = 0.005\ s^{-1}$ for all samples resulting in a *Wi* that falls in the range of 10^{-2}–10^{0} (for low and high M_w samples, respectively) primarily probing entanglement recovery [53]. The theory further predicts that the concentration of open (free, unpaired, unassociated) stickers that have not formed reversible associations (bonds) during self-healing at the interface is given by $c_{open}(t) \approx \frac{1}{R_o^3}(\tau_b/t)$, where $R_o^3 \approx b^3 N^{3/2}$ is the volume of a dangling chain with N monomers. Thus, $c_{open}(t_H) \sim t_H^{-1}$ for time scales $\tau_b < t_H < \tau_{eq}$. At shorter times (less than the Rouse time), the scaling is $t_H^{-3/4}$; however, this cannot be tested with the available experimental data. The regime of $\tau_{eq} < t_H$ in entangled polymers has not been rigorously investigated yet to our knowledge. In the unentangled polymers, equilibrium of c_{open} is reached at $t_H \sim \tau_{eq}$. However, in entangled polymers, c_{open} is dictated by entanglement dynamics and steric constraints, and, therefore, c_{open} may continue to evolve at $\tau_{eq} < t_H$ as equilibrium is reached. The complete reassembly goes by a process of bridge formation (quantified by the surface density of bridges σ_b across the interface) which occur through various self-healing and self-adhesion mechanisms based on values of t_w and εk_bT [22]. In entangled systems, the recovery of associations and entanglements across the interface should be proportional to $1-(\varepsilon_u/\varepsilon_{u,eq})$, where ε_u is the ultimate elongation at healing time t_H and $\varepsilon_{u,eq}$ is the ultimate elongation at the fully recovered state (long times). This function takes the values of 1 for $t_H = 0$ (high concentration of open stickers or low number of interfacial bridges) and approaches 0 at long times (equilibrium concentration of open stickers and many interfacial bridges). The recovery of mechanical properties should follow a power law scaling with t_H as

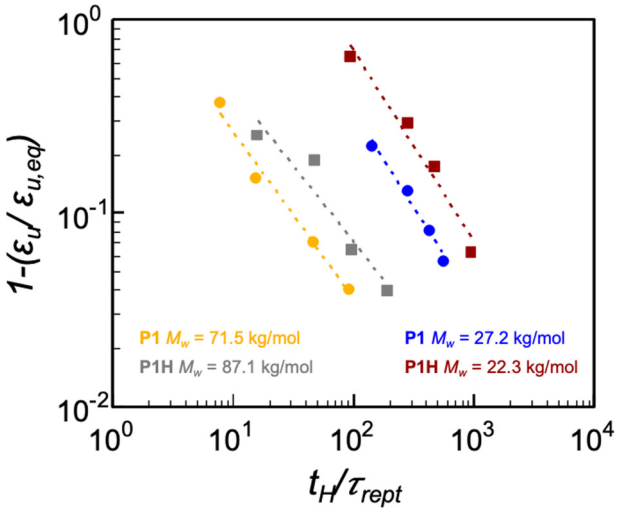

FIG. 11. Kinetics of self-healing at room temperature of four associating polymers of various molecular weight (both **P1** and **P1H** structures) showing the scaling of the concentration of open stickers $c_{open}(t_H) \approx \frac{1}{R_0^3}\left(\frac{\tau_b}{t_H}\right)$ that is proportional to $1-\varepsilon_u/\varepsilon_{u,eq}$ with t_H. Healing timescale is normalized by the reptation time τ_{rep}.

$1-(\varepsilon_u/\varepsilon_{u,eq}) \sim t_H^x$. Figure 11 depicts $1-(\varepsilon_u/\varepsilon_{u,eq})$ as a function t_H for **P1** and **P1H** polymers. Due to the broad relaxation time spectra and the convolution of dynamic timescales, it is difficult to rationalize dynamics with respect to a single relaxation time. However, t_H is normalized by t_{rep} in Fig. 11 to highlight two regimes of healing dynamics based on M_w and importance of entanglement formation where $t_h/\tau_{rep} > 10$. The higher molecular weight polymers exhibit power law scaling of $x \sim -0.8$ at lower values of t_h/τ_{rep}. The slower recovery could be due to delayed diffusion from numerous reversible associations after bond dissociation and reptation occur, convoluted by inhomogeneities caused by potential associative aggregates, especially at the interface. The lower M_w samples follow a more rapid scaling factor of $x \sim -1$. At higher t_h/τ_{rep}, chains have much more respective time to reform entanglements, and the dynamics are favorably balanced with associations to reach enhanced recovery. The difference in healing dynamics between **P1** and **P1R** is modest considering the difference in sticky chain dynamics. Overall, this system with high density of stickers with shorter lifetimes facilitates assisted entanglement reformation to fully recover mechanical properties. The scaling behavior with of $c_{open} \sim t_H^x$ or $\sigma_b \sim t_H^x$ in this new regime of $t_H > \tau_{eq}$ in unexpected as deviations from the theory are expected due to the difference in chain architecture (telechelic vs the pendant associations) and the heavy influence of entanglements. Future work will fully investigate the wider scaling behavior across M_w where for unentangled polymers $c_{open}(t) \sim N^{1/2}$. Such a depencence has not been rigorously determined for entangled systems or architectures with predominatly trapped sticker groups.

The results of the modeling and self-healing dynamics indicate that to fabricate a successful self-healing material, it is essential to have numerous free functional groups at the cut surface without undermining the role of the entanglements. The latter might provide better mechanical properties at the interface although entanglements will slow down the relaxation of chains and thus delay the recovery time for self-healing. The short chain contribution to recovery of mechanical strength is critical for potential adhesion applications. The availability of functional groups ready to interact/associate and quickly connect allows samples to mend and maintain large deformations.

IV. CONCLUSIONS

A series of aminated associating polymers were synthesized by catalytic protocols resulting in polyethylene analogs where every eighth carbon contains a functionalized amine branch. As demonstrated using melt rheology, low T_g coupled with the associative interactions of secondary amines introduces desirable material properties such as tunable rheological properties (liquid-like to gel and soft solid behavior depending on M_w) and autonomously rapid self-healing. The linear viscoelasticity is modeled by a TMA tube-based model to determine molecular parameters such as sticker lifetime and the effective sticky reptation time. The entanglement and association molecular weights (M_e and M_{xx}) are the same for **P1** and **P1H**, where $M_{xx} = 500$ g/mol is approximately equal to two monomer units, resulting in a high number of active associations with respect to the number of entanglements. We find that by changing the polymer backbone chemistry from **P1** to **P1H**, the T_g decreases and the sticky chain dynamics accelerate (τ_s is faster and higher p_{free}). This results in **P1H** showing more relaxation at long timescales compared to **P1** of similar M_w while maintaining comparable entanglement structure and mechanical properties on short timescales. The collection of many fast-associating groups is a rather unexplored regime of self-healing materials. Self-healing dynamics of both **P1** vs **P1H** are evaluated within recent theoretical frameworks for reversible networks. In this regime, both chain and associative timescales must be balanced to enable assisted entanglement reformation and full recovery of mechanical properties. Scaling behavior with healing time, t_H, is identified, but the results further confirm that entanglement dynamics must be included in a future self-healing model. Exceptionally rapid self-healing is observed in low M_w **P1H**, which can fully recover its mechanical properties in 10 min without the influence of external stimuli. The determination of sticky chain timescales provides insight into designing new materials with predictable rheological properties and superior self-healing ability.

ACKNOWLEDGMENTS

NSERC, MITACS, and CREATE Sustainable Synthesis are gratefully acknowledged for funding. The work was supported in part by the Canada Research Chairs program. E.v.R. is Research Associate of the F.R.S.-F.N.R.S.

AUTHOR DECLARATIONS

Conflict of Interest

The authors have no conflicts to disclose.

Author Contributions

B.M.Y, T.T, and D.J.G. contributed equally to this work.

DATA AVAILABILITY

The data that support the findings of this study are available within the article.

REFERENCES

[1] Van Ruymbeke, E., "Preface: Special issue on associating polymers," J. Rheol. **61**(6), 1099–1102 (2017).

[2] Pelton, R., "Polyvinylamine: A tool for engineering interfaces," Langmuir **30**(51), 15373–15382 (2014).

[3] Jiang, H., and F. J. Xu, "Biomolecule-functionalized polymer brushes," Chem. Soc. Rev. **42**(8), 3394–3426 (2013).

[4] Lu, J., and P. H. Toy, "Multifunctional organic polymeric catalysts and reagents," Pure Appl. Chem. **85**(3), 493–587 (2013).

[5] Pinschmidt, R. K., "Polyvinylamine at last," J. Polym. Sci. Part A Polym. Chem. **48**, 2257–2283 (2010).

[6] Verjans, J., A. André, E. Van Ruymbeke, and R. Hoogenboom, "Physically cross-linked polybutadiene by quadruple hydrogen bonding through side-chain incorporation of ureidopyrimidinone with branched alkyl side chains," Macromolecules **55**(3), 928–941 (2022).

[7] Hackelbusch, S., T. Rossow, P. Van Assenbergh, and S. Seiffert, "Chain dynamics in supramolecular polymer networks," Macromolecules **46**(15), 6273–6286 (2013).

[8] Jangizehi, A., M. Ahmadi, and S. Seiffert, "Dynamics of supramolecular associative polymer networks at the interplay of chain entanglement, transient chain association, and chain-sticker clustering," J. Polym. Sci. Part B Polym. Phys. **57**(18), 1209–1223 (2019).

[9] Yount, W. C., H. Juwarker, and S. L. Craig, "Orthogonal control of dissociation dynamics relative to thermodynamics in a main-chain reversible polymer," J. Am. Chem. Soc. **125**(50), 15302–15303 (2003).

[10] Serpe, M. J., and S. L. Craig, "Physical organic chemistry of supramolecular polymers," Langmuir **23**(4), 1626–1634 (2007).

[11] Xu, D., and S. L. Craig, "Scaling laws in supramolecular polymer networks," Macromolecules **44**(13), 5465–5472 (2011).

[12] Hourdet, D., J. A. Gadgil, K. Podhajecka, M. V. Badiger, A. Brûlet, and P. P. Wadgaonkar, "Thermoreversible behavior of associating polymer solutions: Thermothinning versus thermothickening," Macromolecules **38**(20), 8512–8521 (2005).

[13] Nair, K. P., V. Breedveld, and M. Weck, "Complementary hydrogen-bonded thermoreversible polymer networks with tunable properties," Macromolecules **41**(10), 3429–3438 (2008).

[14] David, R. L. A. *et al*., "Effects of pairwise, donor-acceptor functional groups on polymer solubility, solution viscosity and mist control," Macromolecules **42**, 1380–1391 (2009).

[15] Nair, K. P., V. Breedveld, and M. Weck, "Modulating mechanical properties of self-assembled polymer networks by multi-functional complementary hydrogen bonding," Soft Matter **7**(2), 553–559 (2011).

[16] Golkaram, M., and K. Loos, "A critical approach to polymer dynamics in supramolecular polymers," Macromolecules **52**(24), 9427–9444 (2019).

[17] Shabbir, A., H. Goldansaz, O. Hassager, E. Van Ruymbeke, and N. J. Alvarez, "Effect of hydrogen bonding on linear and nonlinear rheology of entangled polymer melts," Macromolecules **48**(16), 5988–5996 (2015).

[18] Ahmadi, M., A. Jangizehi, E. Van Ruymbeke, and S. Seiffert, "Deconvolution of the effects of binary associations and collective assemblies on the rheological properties of entangled side-chain supramolecular polymer networks," Macromolecules **52**(14), 5255–5267 (2019).

[19] Jangizehi, A., S. R. Ghaffarian, W. Schmolke, and S. Seiffert, "Dominance of chain entanglement over transient sticking on chain dynamics in hydrogen-bonded supramolecular polymer networks in the melt," Macromolecules **51**(8), 2859–2871 (2018).

[20] Ahmadi, M., L. G. D. Hawke, H. Goldansaz, and E. Van Ruymbeke, "Dynamics of entangled linear supramolecular chains with sticky side groups: Influence of hindered fluctuations," Macromolecules **48**(19), 7300–7310 (2015).

[21] Gilmour, D. J. *et al*., "Catalytic amine functionalization and polymerization of cyclic alkenes creates adhesive and self-healing materials," ACS Appl. Polym. Mater. **3**(5), 2330–2335 (2021).

[22] Stukalin, E. B., L. H. Cai, N. A. Kumar, L. Leibler, and M. Rubinstein, "Self-healing of unentangled polymer networks with reversible bonds," Macromolecules **46**(18), 7525–7541 (2013).

[23] Cates, M. E., "Reptation of living polymers: Dynamics of entangled polymers in the presence of reversible chain-scission reactions," Macromolecules **20**(9), 2289–2296 (1987).

[24] Leibler, L., M. Rubinstein, and R. H. Colby, "Dynamics of reversible networks," Macromolecules **24**(16), 4701–4707 (1991).

[25] Hawke, L. G. D., M. Ahmadi, H. Goldansaz, and E. Van Ruymbeke, "Viscoelastic properties of linear associating poly(n-butyl acrylate) chains," J. Rheol. **60**(2), 297–310 (2016).

[26] Van Ruymbeke, E., R. Keunings, and C. Bailly, "Prediction of linear viscoelastic properties for polydisperse mixtures of entangled star and linear polymers: Modified tube-based model and comparison with experimental results," J. Non-Newtonian Fluid Mech. **128**, 7–22 (2005).

[27] Singh, S., and C. N. R. Rao, "Spectroscopic studies of self-association due to hydrogen bonding," J. Phys. Chem. **71**(4), 1074–1078 (1967).

[28] Lewis, C. L., K. Stewart, and M. Anthamatten, "The influence of hydrogen bonding side-groups on viscoelastic behavior of linear and network polymers," Macromolecules **47**(2), 729–740 (2014).

[29] Snijkers, F., and D. Vlassopoulos, "Cone-partitioned-plate geometry for the ARES rheometer with temperature control," J. Rheol. **55**(6), 1167–1186 (2011).

[30] Ebrahimi, M., V. K. Konaganti, and S. G. Hatzikiriakos, "Dynamic slip of polydisperse linear polymers using partitioned plate," Phys. Fluids **30**, 030601 (2018).

[31] Konaganti, V. K., M. Derakhshandeh, M. Ebrahimi, E. Mitsoulis, and S. G. Hatzikiriakos, "Non-isothermal extrudate swell," Phys. Fluids **28**, 123101 (2016).

[32] Tomkovic, T., and S. G. Hatzikiriakos, "Nonlinear rheology of poly(ethylene-co-methacrylic acid) ionomers," J. Rheol. **62**(6), 1319–1329 (2018).

[33] Sentmanat, M. L., "Miniature universal testing platform: From extensional melt rheology to solid-state deformation behavior," Rheol. Acta **43**(6), 657–669 (2004).

[34] Dealy, J. M., D. J. Read, and R. G. Larson, *Structure and Rheology of Molten Polymers: From Structure to Flow Behavior and Back Again* (Springer, Cincinnati, 2018).

[35] Semenov, A. N., and M. Rubinstein, "Thermoreversible gelation in solutions of associative polymers. 2. Linear dynamics," Macromolecules **31**(4), 1373–1385 (1998).

[36] Rubinstein, M., and A. N. Semenov, "Dynamics of entangled solutions of associating polymers," Macromolecules **34**(4), 1058–1068 (2001).

[37] Shabbir, A. *et al*., "Nonlinear shear and uniaxial extensional rheology of polyether-ester-sulfonate copolymer ionomer melts," J. Rheol. **61**(6), 1279–1289 (2017).

[38] Zhang, Z., Q. Chen, and R. H. Colby, "Dynamics of associative polymers," Soft Matter **14**(16), 2961–2977 (2018).

[39] Chen, Q., Z. Zhang, and R. H. Colby, "Viscoelasticity of entangled random polystyrene ionomers," J. Rheol. **60**(6), 1031–1040 (2016).

[40] Fetters, L. J., D. J. Lohse, and R. H. Colby, "Chain dimensions and entanglement spacings," in *Physical Properties of Polymers Handbook* (Springer, New York, 2006), pp. 445–452.

[41] Baral, S. *et al*., "Single-chain polymerization dynamics and conformational mechanics of conjugated polymers," Chem **7**(8), 2175–2189 (2021).

[42] Winter, H. H., "Three views of viscoelasticity for Cox-Merz materials," Rheol. Acta **48**(3), 241–243 (2009).

[43] Van Ruymbeke, E., C. Bailly, R. Keunings, and D. Vlassopoulos, "A general methodology to predict the linear rheology of branched polymers," Macromolecules **39**(18), 6248–6259 (2006).

[44] Chen, Q., G. J. Tudryn, and R. H. Colby, "Ionomer dynamics and the sticky Rouse model," J. Rheol. **57**(5), 1441–1462 (2013).

[45] Yount, W. C., D. M. Loveless, and S. L. Craig, "Small-molecule dynamics and mechanisms underlying the macroscopic mechanical properties of coordinatively cross-linked polymer networks," J. Am. Chem. Soc. **127**(41), 14488–14496 (2005).

[46] Sprakel, J., J. Van Der Gucht, M. A. Cohen Stuart, and N. A. M. Besseling, "Brownian particles in transient polymer networks," Phys. Rev. E **77**(6), 061502 (2008).

[47] Van Ruymbeke, E. *et al*., "Entangled dendritic polymers and beyond: Rheology of symmetric Cayley-tree polymers and macromolecular self-assemblies," Macromolecules **40**(16), 5941–5952 (2007).

[48] Kuanr, N. *et al*., "Dynamic cross-linking of catalytically synthesized poly(aminonorbornenes)," Macromolecules **53**(7), 2649–2661 (2020).

[49] Hohl, D. K., A. C. Ferahian, L. Montero De Espinosa, and C. Weder, "Toughening of glassy supramolecular polymer networks," ACS Macro Lett. **8**(11), 1484–1490 (2019).

[50] Liu, M., P. Liu, G. Lu, Z. Xu, and X. Yao, "Multiphase-assembly of siloxane oligomers with improved mechanical strength and water-enhanced healing," Angew. Chem. **130**(35), 11412–11416 (2018).

[51] Wu, D. Y., S. Meure, and D. Solomon, "Self-healing polymeric materials: A review of recent developments," Prog. Polym. Sci. **33**(5), 479–522 (2008).

[52] Hager, M. D., P. Greil, C. Leyens, S. Van Der Zwaag, and U. S. Schubert, "Self-healing materials," Adv. Mater. **22**, 5424–5430 (2010).

[53] Hinton, Z. R., A. Shabbir, and N. J. Alvarez, "Dynamics of supramolecular self-healing recovery in extension," Macromolecules **52**(6), 2231–2242 (2019).

[54] Cordier, P., F. Tournilhac, C. Soulié-Ziakovic, and L. Leibler, "Self-healing and thermoreversible rubber from supramolecular assembly," Nature **451**(7181), 977–980 (2008).

[55] Sbrescia, S., J. Ju, T. Engels, E. Van Ruymbeke, and M. Seitz, "Morphological origins of temperature and rate dependent mechanical properties of model soft thermoplastic elastomers," J. Polym. Sci. **59**(6), 477–493 (2021).